Polarized micro-Raman scattering characterization of Mg_2Si nanolayers in (001) Si matrix

2007 J. Phys.: Condens. Matter 19 086220

(http://iopscience.iop.org/0953-8984/19/8/086220)

IOP PUBLISHING JOURNAL OF PHYSICS: CONDENSED MATTER

J. Phys.: Condens. Matter **19** (2007) 086220 (9pp) doi:10.1088/0953-8984/19/8/086220

Polarized micro-Raman scattering characterization of Mg_2Si nanolayers in (001) Si matrix

G Zlateva[1], A Atanassov[2], M Baleva[2], L Nikolova[3] and M V Abrashev[2]

[1] Department of Physics and Biophysics, Medical University, 2 Zdrave Street, 1431 Sofia, Bulgaria
[2] Faculty of Physics, Sofia University, 5 J Boucher Boulevard, 1164 Sofia, Bulgaria
[3] Department of Applied Physics, Technical University of Sofia, 8 Kliment Ohridski Street, 1000 Sofia, Bulgaria

E-mail: baleva@phys.uni-sofia.bg

Received 13 December 2006, in final form 11 January 2007
Published 9 February 2007
Online at stacks.iop.org/JPhysCM/19/086220

Abstract

An orientational growth of the Mg_2Si lattice relative to the Si lattice is considered assuming minimum mismatch of their lattice parameters. The Raman scattering cross-sections are calculated for the four possible orientations of the Mg_2Si lattice positioned in this way. The integral intensity ratios for the F_{2g} mode of Mg_2Si in different polarization configurations, obtained from the experimental spectra, are compared with the calculated ratios.

It is found that the Mg_2Si nanolayer's morphology is sensitive to the implantation energy, which determines both the peak Mg concentration in the initial implantation profile and its position in the sample depth. At a peak concentration of the order of the stoichiometric concentration, the layers are highly oriented. When the peak concentration is higher and the peak is placed closer to the surface, the layers are polycrystalline.

1. Introduction

A variety of techniques have been developed for the fabrication of nanostructures in or on substrates. These techniques can be technologically distinguished on the basis of the dominant physical and chemical processes involved—diffusion synthesis, ion-beam synthesis, and atomic and molecular deposition. The appropriate technology is not universal; it depends on the materials properties. It is shown that nanolayers and precipitates of the semiconducting metal silicide Mg_2Si in a Si matrix can be prepared successfully by ion-beam synthesis (IBS) [1].

The prospects of the application of a heterostructure in silicon-based optoelectronics and nanoelectronics depend on the epitaxial relationships between monocrystalline silicon and the semiconductor, Mg_2Si in particular. For good-quality epitaxial formations, the lattice mismatch between the silicide and the silicon matrix is typically less than 3% [2].

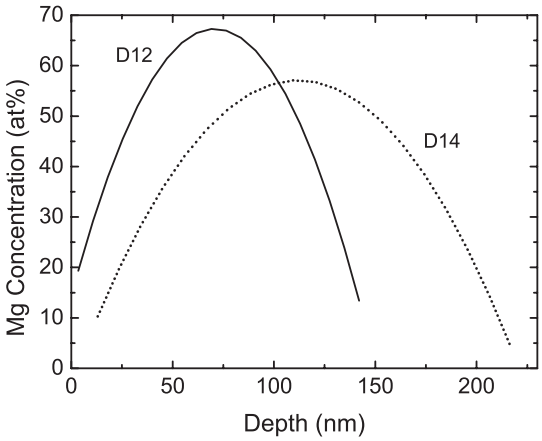

Figure 1. Mg implantation profiles, simulated by *stopping and range of ions in matter*.

Similarly to Si, Mg_2Si has cubic structure, but with a larger lattice parameter $a = 0.6351$ nm [3]. The mismatch between Si and Mg_2Si lattices in the (111) Si and (111) Mg_2Si planes is as small as 1.3% when their unit cells are rotated by 30° to each other around the [111] direction [4]. The good match of the geometrical lattices is never the only sufficient condition for high-quality epitaxy. In general, the chemistry at the interface plays a major role. In the case of IBS, however, epitaxial growth has to depend mainly on the lattice match. Then, high-quality epitaxial growth of the Mg_2Si phase in Si matrix is expected.

Polarized Raman scattering appears to be a powerful tool for the investigation of the quality of the orientational growth. In this work, the scattered light intensity ratios for different polarization configurations are calculated, assuming the smallest mismatch between the Si and Mg_2Si unit cells. The calculated ratios are compared with the experimentally obtained ratios and conclusions about the influence of the technological parameters are drawn.

2. Experimental part and results

The samples were prepared by IBS, followed by rapid thermal annealing. The mass-separated $^{24}Mg^{+}$ ions were implanted into (001) Si wafers. The dose of the implanted Mg ions was 8×10^{17} cm^{-2}. The implantation was performed with two different energies: 40 keV for sample D12 and 60 keV for sample D14. The annealing temperature and the time for both types of samples were the same: 500 °C and 600 s. The Mg implantation profiles, simulated by *stopping and range of ions in matter*, are shown in figure 1. It is seen from the figure that the Mg concentration is lower than the Mg_2Si stoichiometric concentration (66.66 at.% Mg) for samples implanted at higher energy (sample D14) and exceeds that for the samples implanted at lower energy (sample D12). It is also seen that the peak concentration in the samples, implanted at lower energy, is placed closer to the sample surface.

The surface morphology of the samples was examined using a Jeol JSM-840A scanning electron microscope (SEM). In figure 2 the SEM micrographs of samples D12 and D14, annealed for the same time (30 s), are given. On the surface of sample D12, prepared at lower implantation energy and with the Mg atom peak concentration closer to the sample surface, the dendrites are seen, while only a skeleton structure is observed on the surface of the sample, prepared at the higher implantation energy. Nevertheless, the samples under investigation were

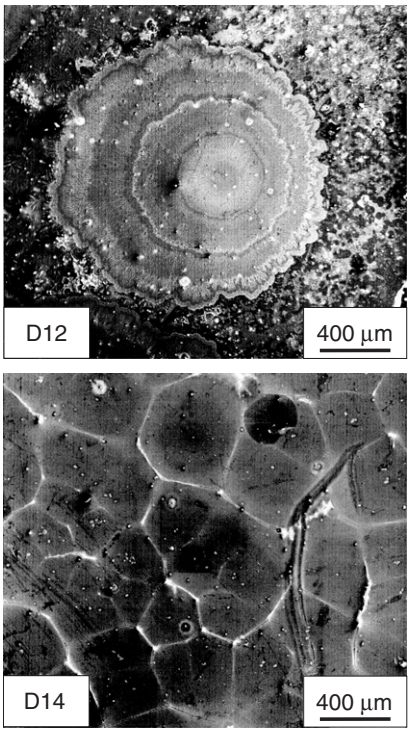

Figure 2. SEM micrographs of samples D12 and D14, annealed for 30 s.

annealed for a longer time; one can conclude from figure 2 that the quantity of the unreacted Mg atoms, reaching the surface of sample D14, is much lower.

The polarized micro-Raman spectra between 200 and 500 cm^{-1} were measured at room temperature using a triple multichannel spectrometer, Microdil 28 (Dilor), equipped with an optical microscope (objective $\times 100$; NA $= 0.95$) for focusing the incident laser beam (Ar^+ laser; $\lambda = 488.0$ nm; PL ≈ 13 mW on the sample; focus spot diameter about 2–3 μm). The scattered light was collected in the backward-scattering geometry.

The orientation of the incident light polarization was chosen along the edge of the Si precursor, which coincides with the [110] or [1$\bar{1}$0] directions in the Si-crystal (x- and y-directions, respectively). The polarized Raman spectra of samples D12 and D14 were measured both in parallel, $(c(xx)\bar{c})$ and $(c(yy)\bar{c})$, and in the $(c(xy)\bar{c})$ crossed polarizations of the incident and scattered light (c stands for the [001] direction in the Si crystal) and are shown in figure 3.

The semiconductor Mg_2Si belongs to the cubic system with space group $Fm\bar{3}m$ (O_h^5). The material has three atoms in the primitive unit cell, and therefore six optical branches in the vibrational dispersion curves at the centre of the Brillouin zone are allowed. According to factor-group analysis, the optical phonon modes with wavevector $\vec{k} \approx 0$ are triply degenerate, corresponding to F_{2g} and F_{1u} irreducible representations. Because of the inversion symmetry, the F_{2g} and F_{1u} modes are Raman-active and infrared-active, respectively. Due to the macroscopic electric field, the F_{1u} mode splits into a doubly degenerate transverse optic (TO) mode and a longitudinal optic (LO) mode.

The theoretical calculations give for the frequency of the triply degenerate Raman-allowed F_{2g} mode the value 258 cm^{-1} [5, 6]. Another sharp line, assigned to Fröhlich-interaction-

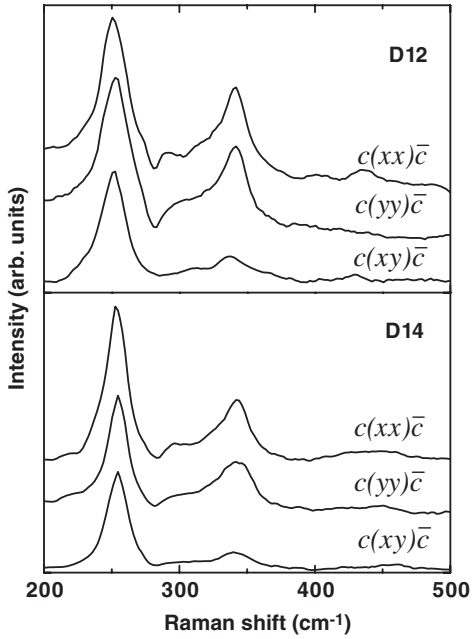

Figure 3. Polarized micro-Raman spectra in parallel ($c(xx)\bar{c}$) and ($c(yy)\bar{c}$) and in crossed ($c(xy)\bar{c}$) polarizations of incident and scattered light, obtained for samples D12 and D14.

induced scattering by the Raman-inactive F_{1u} (LO)-mode, is usually observed at 345–348 cm^{-1} in the Raman spectra of Mg_2Si [7–10]. Thus, the peaks at 256 and 345 cm^{-1}, observed in our experimental spectra, are related to the F_{2g} and the F_{1u} (LO) modes of the Mg_2Si. The peak at 345 cm^{-1} is much weaker in the crossed polarization configuration, which is quite reasonable if one takes into account that it is concluded to be mainly diagonal [11].

3. Discussion

In order to obtain information about the orientational growth of the Mg_2Si phase, the Raman cross-sections in the different polarization configurations have to be calculated. For this purpose, a transformation of the polarization directions from the (001) Si coordinate system to the Mg_2Si system in a condition of smallest mismatch has to be performed.

3.1. Transformation tensors

The smallest mismatch between Si and Mg_2Si unit cells can be obtained at a mapping of the (111) Si and (111) Mg_2Si planes and a rotation of the Si and Mg_2Si unit cells by 30° to each other around the [111] direction. The polarized Raman spectra were measured relative to the [110] and [1$\bar{1}$0] directions on the surface of the Si monocrystalline matrix (x and y directions). The calculation of the Raman intensity ratios for the Mg_2Si lattice in different polarization configurations has to be performed for the corresponding Mg_2Si directions. Then the transformation tensor of the unit vectors $\vec{e}_x$, $\vec{e}_y$ and $\vec{e}_z$ of the Si lattice into the unit vectors $\vec{e}'_x$, $\vec{e}'_y$ and $\vec{e}'_x$ in the Mg_2Si lattice can be calculated by the use of the two direction transformations and of the condition for an orthogonality of the coordinate system's cosine directories. There

are four possible orientations of the Mg_2Si lattice in the Si matrix at the condition for smallest mismatch. The four corresponding transformation tensors, labelled T_1, T_2, T_3 and T_4, were worked out. As an example, the detailed calculations of the tensor T_1 are given. The tensor has to transform the [011] Si direction into the $[\bar{1}12]$ Mg_2Si direction and the [121] Si direction into the [011] Mg_2Si direction. In other words, the unit vector $(0, \frac{1}{\sqrt{2}}, \frac{1}{\sqrt{2}})$ of the [011] Si moves to the unit vector $(-\frac{1}{\sqrt{6}}, \frac{1}{\sqrt{6}}, \frac{2}{\sqrt{6}})$ of the $[\bar{1}12]$ Mg_2Si and the unit vector $(\frac{1}{\sqrt{6}}, \frac{2}{\sqrt{6}}, \frac{2}{\sqrt{6}})$ of the [121] Si moves to the unit vector $(0, \frac{1}{\sqrt{2}}, \frac{1}{\sqrt{2}})$ of the [011] Mg_2Si. The tensor elements α_{ij} can be calculated from the relations:

$$\begin{pmatrix} \alpha_{11} & \alpha_{12} & \alpha_{13} \\ \alpha_{21} & \alpha_{22} & \alpha_{23} \\ \alpha_{31} & \alpha_{32} & \alpha_{33} \end{pmatrix} \begin{pmatrix} 0 \\ \frac{1}{\sqrt{2}} \\ \frac{1}{\sqrt{2}} \end{pmatrix} = \begin{pmatrix} -\frac{1}{\sqrt{6}} \\ \frac{1}{\sqrt{6}} \\ \frac{2}{\sqrt{6}} \end{pmatrix}$$

and

$$\begin{pmatrix} \alpha_{11} & \alpha_{12} & \alpha_{13} \\ \alpha_{21} & \alpha_{22} & \alpha_{23} \\ \alpha_{31} & \alpha_{32} & \alpha_{33} \end{pmatrix} \begin{pmatrix} \frac{1}{\sqrt{6}} \\ \frac{2}{\sqrt{6}} \\ \frac{1}{\sqrt{6}} \end{pmatrix} = \begin{pmatrix} 0 \\ \frac{1}{\sqrt{2}} \\ \frac{1}{\sqrt{2}} \end{pmatrix}.$$

The well-known orthogonality relations of the tensor elements are:

$$\alpha_{ij}\alpha_{jk} = \delta_{ik}, \qquad i, j, k = 1, 2, 3.$$

The obtained tensor is:

$$T_1 = \begin{pmatrix} \frac{1}{\sqrt{3}} - \frac{1}{3} & \frac{1}{3} & -\frac{1}{\sqrt{3}} - \frac{1}{3} \\ \frac{1}{\sqrt{3}} + \frac{1}{3} & \frac{1}{\sqrt{3}} - \frac{1}{3} & \frac{1}{3} \\ -\frac{1}{3} & \frac{1}{\sqrt{3}} + \frac{1}{3} & \frac{1}{\sqrt{3}} - \frac{1}{3} \end{pmatrix}.$$

The remaining three tensors are obtained analogically and have the forms:

$$T_2 = \begin{pmatrix} \frac{1}{\sqrt{3}} - \frac{1}{3} & \frac{1}{\sqrt{3}} + \frac{1}{3} & \frac{1}{3} \\ \frac{1}{3} & \frac{1}{\sqrt{3}} - \frac{1}{3} & -\frac{1}{\sqrt{3}} - \frac{1}{3} \\ \frac{1}{\sqrt{3}} + \frac{1}{3} & -\frac{1}{3} & \frac{1}{\sqrt{3}} - \frac{1}{3} \end{pmatrix},$$

$$T_3 = \begin{pmatrix} \frac{1}{\sqrt{3}} + \frac{1}{3} & -\frac{1}{\sqrt{3}} + \frac{1}{3} & -\frac{1}{3} \\ \frac{1}{3} & \frac{1}{\sqrt{3}} + \frac{1}{3} & \frac{1}{\sqrt{3}} - \frac{1}{3} \\ \frac{1}{\sqrt{3}} - \frac{1}{3} & -\frac{1}{3} & \frac{1}{\sqrt{3}} + \frac{1}{3} \end{pmatrix},$$

$$T_4 = \begin{pmatrix} -\frac{1}{\sqrt{3}} - \frac{1}{3} & \frac{1}{\sqrt{3}} - \frac{1}{3} & -\frac{1}{3} \\ -\frac{1}{3} & -\frac{1}{\sqrt{3}} - \frac{1}{3} & \frac{1}{\sqrt{3}} - \frac{1}{3} \\ \frac{1}{\sqrt{3}} - \frac{1}{3} & -\frac{1}{3} & -\frac{1}{\sqrt{3}} - \frac{1}{3} \end{pmatrix}.$$

In figure 4 the embedding of Mg_2Si lattice into the Si lattice, described by tensor T_1, is illustrated. The tensor transforms the coordinate system of the Si lattice with unit vectors $\vec{e}_x$, $\vec{e}_y$ and $\vec{e}_z$ into the system with unit vectors $\vec{e}'_x$, $\vec{e}'_y$ and $\vec{e}'_z$ of the Mg_2Si lattice. Then the directions [110], [011] and $[\bar{1}01]$ in Si map respectively the directions [121], $[\bar{1}12]$ and $[\bar{2}\bar{1}1]$ in Mg_2Si.

It is worth mentioning that the tensors T_1 and T_2 transform the [110] Si direction (x-direction) into the $Mg_2Si(111)$ plane, but the $[1\bar{1}0]$ Si direction—out of the plane in direction, which in the case of T_1 and T_2 are given by the unit vectors $(\frac{2}{3\sqrt{2}} - \frac{1}{\sqrt{6}}, -\frac{2}{3\sqrt{2}}, \frac{2}{3\sqrt{2}} + \frac{1}{\sqrt{6}})$ and $(\frac{2}{3\sqrt{2}}, \frac{1}{\sqrt{6}} - \frac{2}{3\sqrt{2}}, -\frac{1}{\sqrt{6}} - \frac{2}{3\sqrt{2}})$, respectively.

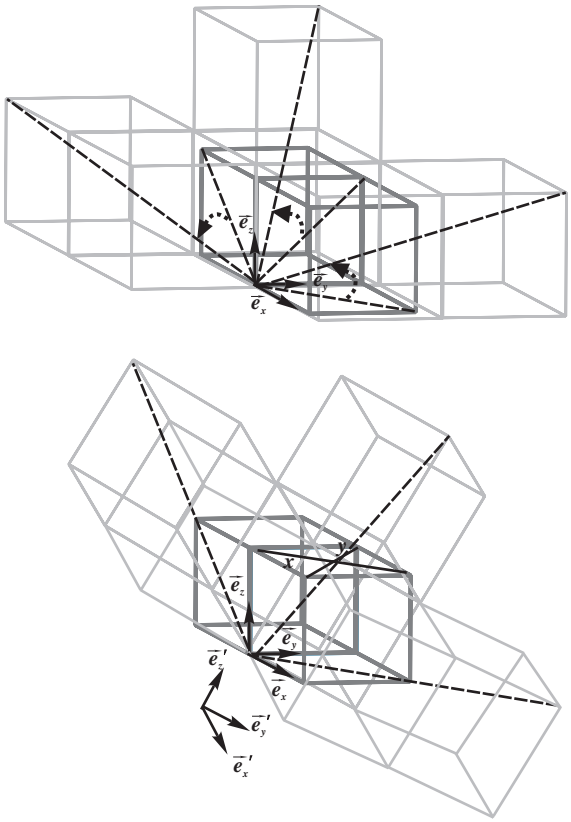

Figure 4. Transformation of the coordinate system of the Si unit cell (thicker lines) with unit vectors $\vec{e}_x$, $\vec{e}_y$ and $\vec{e}_z$ into the system of the Mg_2Si lattice with unit vectors $\vec{e}'_x$, $\vec{e}'_y$ and $\vec{e}'_z$, described by transformation tensor T_1. The x and y directions in Si cell are drawn.

The Raman intensity ratios calculated with these two tensors turn to be equal and therefore the Mg_2Si lattice orientations, described by these tensors, appeared to be equivalent.

Analogically, the tensors T_3 and T_4 transform the $[1\bar{1}0]$ Si direction (y-direction) into a direction lying in the $Mg_2Si(111)$ plane, while the [110] Si direction is transformed into directions with unit vectors $(\frac{2}{3\sqrt{2}}, \frac{1}{\sqrt{6}} + \frac{2}{3\sqrt{2}}, \frac{1}{\sqrt{6}} - \frac{2}{3\sqrt{2}})$ and $(-\frac{2}{3\sqrt{2}}, -\frac{1}{\sqrt{6}} - \frac{2}{3\sqrt{2}}, \frac{1}{\sqrt{6}} - \frac{2}{3\sqrt{2}})$, respectively. The orientations of the Mg_2Si lattice, described by these two tensors, are equivalent as well.

The embedding of the Mg_2Si lattice in the Si matrix on the assumption of smallest mismatch is illustrated in figure 5. The Mg_2Si lattice with the same orientation forms densely packed layer.

3.2. Raman intensity ratios

The scattered intensities of the Mg_2Si Raman-active F_{2g} mode for the different scattering configurations were calculated using the relation:

$$I_s \propto \sum_j \left| e_i R_j e_s \right|^2 ,$$

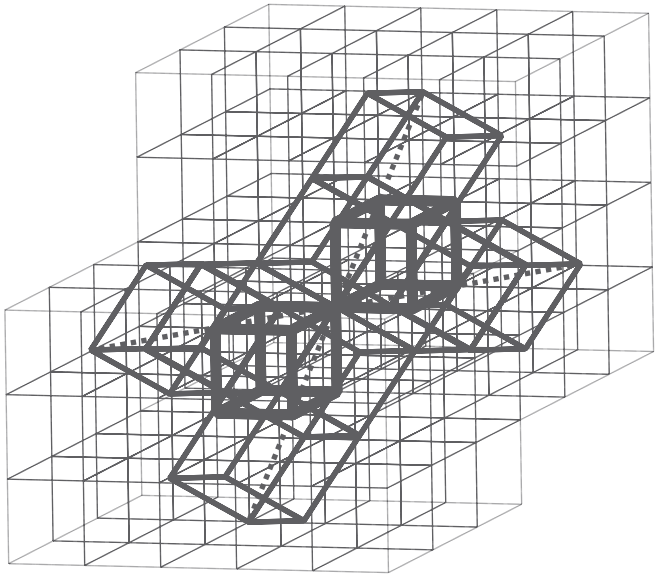

Figure 5. The embedding of eight Mg_2Si unit cells in the Si matrix on the assumption of the smallest mismatch.

Table 1. The calculated Raman integral intensity ratios for different polarization configurations and for different orientations of the Mg_2Si lattice in the Si matrix.

	Intensity ratio		
Transformation tensor	$\frac{I_{c(xx)\bar{c}}}{I_{c(yy)\bar{c}}}$	$\frac{I_{c(xy)\bar{c}}}{I_{c(xx)\bar{c}}}$	$\frac{I_{c(yx)\bar{c}}}{I_{c(yy)\bar{c}}}$
T_1	1.42	0.44	0.63
T_2	1.42	0.44	0.63
T_3	0.70	0.63	0.44
T_4	0.70	0.63	0.44

where the unit vectors e_i and e_s indicate the polarization directions of the incident and scattered light, respectively, and R_j are the Raman tensor elements.

The intensity ratios for different polarization configurations were calculated using the transformed unit vectors in Mg_2Si for the polarization directions of incident and scattered light and the Raman tensors for the F_{2g} mode, being

$$R_1 = \begin{pmatrix} 0 & b & 0 \\ b & 0 & 0 \\ 0 & 0 & 0 \end{pmatrix}, \qquad R_2 = \begin{pmatrix} 0 & 0 & b \\ 0 & 0 & 0 \\ b & 0 & 0 \end{pmatrix}, \qquad R_3 = \begin{pmatrix} 0 & 0 & 0 \\ 0 & 0 & b \\ 0 & b & 0 \end{pmatrix}.$$

The theoretically calculated intensity ratios for different orientations of the Mg_2Si lattice relative to the Si matrix, described by tensors T_1, T_2, T_3, and T_4 respectively, are given in table 1.

The integral intensities of the peak assigned to the F_{2g} mode were calculated from the experimental Raman spectra, taken in different polarization configurations, and are shown in figure 3. The intensity ratios $\frac{I_{c(xx)\bar{c}}}{I_{c(yy)\bar{c}}}$, $\frac{I_{c(xy)\bar{c}}}{I_{c(xx)\bar{c}}}$ and $\frac{I_{c(yx)\bar{c}}}{I_{c(yy)\bar{c}}}$ were then obtained. In table 2 the experimentally obtained ratios are compared with the theoretically calculated ratios. As is seen from the table, the agreement between the theoretically calculated and experimentally obtained ratios is sufficiently good in the case of sample D14. The latter implies the formation of a more

Table 2. Comparison of the experimentally obtained ratios with the calculated ones.

	Intensity ratio					
	$\frac{I_{c(xx)\bar{c}}}{I_{c(yy)\bar{c}}}$		$\frac{I_{c(xy)\bar{c}}}{I_{c(xx)\bar{c}}}$		$\frac{I_{c(yx)\bar{c}}}{I_{c(yy)\bar{c}}}$	
Sample	Calculated	Experiment	Calculated	Experiment	Calculated	Experiment
D12		1.12		0.61		0.71
	1.42		0.44		0.63	
D14		1.47		0.45		0.66

or less densely packed continuous or quasi-continuous layer. It may also be concluded from the comparison of the intensity ratios that the predominant orientation of the Mg_2Si phase is that described by one of the two possible transformations T_1 or T_2.

In the case of the samples produced at the lower implantation energy (D12), the experimentally obtained ratios cannot be related to any one of the possible theoretically calculated ratios. The latter indicates that the Mg_2Si phase in these samples is present in the form of crystalline grains with no predominant orientation. In accord with this, dendrites are observed on the surface of sample D12, as is seen from figure 2. The dendrites' growth can be understood if one takes into account the following. On annealing, along with nucleation of the Mg_2Si phase, the diffusion of unreacted Mg atoms takes place. The Mg atom's diffusion coefficient in the region closer to the surface is enhanced by the vacancy mechanism. The closer to the surface, the higher the density of the vacancies created during implantation. In the samples produced at lower implantation energy (D12), the peak concentration in the initial profile is even higher than the stoichiometric concentration and the peak is placed close to the surface. Then a broadening of the stoichiometric region to the sample surface is to be expected. The formation of the Mg_2Si phase leads to a strong expansion of the region due to the lower value of the Mg_2Si bulk density. The thickness of the resulting Mg_2Si layer, d_{Mg_2Si}, if a Si layer with a thickness d_{Si} is consumed during the reaction, is estimated from the mass ratio and the bulk densities of Si, Mg and Mg_2Si, and we obtained $d_{Mg_2Si} = 3.2d_{Si}$–$3.39d_{Si}$. The strong expansion favours the dendrites' formation. The peak concentration in the initial profile of the samples produced at higher implantation energy (D14) is lower and the peak is deeper in the sample. Then the number of unreacted atoms is limited and only skeletons are seen on these sample surfaces. The predominant quantity of the implanted Mg atoms reacts with the Si atoms in the substrate depth. Due to the influence of the oriented substrate, oriented continuous or quasi-continuous buried Mg_2Si layers are formed.

4. Conclusions

The Raman scattering cross-sections in the four possible orientations of the Mg_2Si lattice in the (001) Si matrix were calculated, with the assumption of minimum mismatch of their parameters. The integral intensity ratios for the F_{2g} mode in different polarization configurations obtained from the experimental spectra were compared with the calculated spectra. It was found that the Mg_2Si nanolayer's morphology is sensitive to the implantation energy, which determines both the peak concentration of the implanted ions and its position. At a peak concentration of the order of the stoichiometric concentration and with the peak placed deeper in the sample's depth, the layers are highly oriented. When the peak concentration is higher and the peak is placed closer to the surface, the layers are polycrystalline due to the formation of dendrites on the sample surface.

Acknowledgments

This work is supported by the National Fund for Scientific Investigations, contract number Φ1301/03, by the Sofia University Fund for Scientific Investigations, contract number 67, and by the French–Bulgarian bilateral Programme PAI-RILA 2/5.

References

[1] Goranova E, Amov B, Baleva M, Trifonova E P and Jordanov P 2004 *J. Mater. Sci.* **39** 1857
[2] Clevenger L A and Mann R W 1995 *Properties of Metal Silicides* ed K Maex and M Vom Rossum (London: INSPEC, IEE) pp 61–70
[3] LaBotz R J, Mason D R and O'Kane D F 1963 *J. Electrochem. Soc.* **110** 127
[4] Wigren C, Andersen J N and Nyholm R 1993 *Surf. Sci.* **289** 290
[5] Whitten W B, Chung P L and Danielson G C 1965 *J. Phys. Chem. Solids* **26** 49
[6] Baranek P H and Schamps J 1997 *J. Phys. Chem.* B **101** 9147
[7] Laughman L and Davis L W 1971 *Solid State Commun.* **9** 497
[8] Baleva M, Zlateva G, Atanassov A, Abrashev M and Goranova E 2005 *Phys. Rev.* B **72** 115330
[9] Atanassov A, Zlateva G, Baleva M, Goranova E, Amov B, Angelov Ch and Mikli V 2006 *Plasma Process. Polym.* **3** 219
[10] Zlateva G, Atanassov A, Baleva M and Nikolova L 2006 *Plasma Process. Polym.* **3** 224
[11] Onari S and Cardona M 1976 *Phys. Rev.* B **14** 3520